INTERNATIONAL JOURNAL OF AUTOMOTIVE AND MECHANICAL ENGINEERING
ISSN: 2229-8649 e-ISSN: 2180-1606
VOLUME 22, ISSUE 3, 2025, 12547 - 12559
DOI: https://doi.org/10.15282/ijame.22.3.2025.1.0958

RESEARCH ARTICLE

Impact of Surface Roughness on Interference Resistance in Delft 372 Catamarans

Ahmad Firdhaus, Kiryanto*, Ahmad Fauzan Zakki, Muhammad Luqman Hakim, Husein Khalis

Department of Naval Architecture, Faculty of Engineering, Diponegoro University, Semarang, Central Java, 50221, Indonesia

ABSTRACT – Surface roughness from marine biofouling significantly compromises catamaran performance, yet current models fail to predict its speed-dependent interference effects, a critical gap in sustainable vessel design. This study employs validated Reynolds-averaged Navier-Stokes-based computational fluid dynamics with the k-ω Shear Stress Transport turbulence model to quantify hydrodynamic impacts across Froude numbers ranging from 0.1 to 0.8. Four different biofouling conditions were systematically analyzed, with rigorous experimental validation against towing-tank data. Key results demonstrate that heavy fouling increased total resistance by 35% at Fr 0.8 versus hydrodynamically smooth surfaces, yet paradoxically generated favorable interference, IF = -0.08, through turbulence-mediated wave suppression. Conversely, hydraulically smooth surfaces exhibited peak detrimental interference, IF = 0.15, at Fr 0.5 due to constructive wave reinforcement. Concurrently, the heavy slime surface reduced inter-hull wave amplitude by 14.5% at Fr 0.5, while expanding the wetted area by 1.24%. The findings address the biofouling paradox by demonstrating that surface roughness facilitates a net reduction in resistance at Fr ≥ 0.65, challenging traditional beliefs regarding the uniformly negative impact of fouling. This study presents the inaugural predictive framework for strategic fouling management, emphasizing bow and midship interference zones, thereby addressing a significant gap in hydrodynamic prediction within realistic operational contexts.

ARTICLE HISTORY
Received : 09th Aug. 2024
Revised : 19th May 2025
Accepted : 03rd July 2025
Published : 01st Sept. 2025

KEYWORDS
Catamaran
Ship resistance
Interference factor
Surface roughness
Computational fluid dynamics

1. INTRODUCTION

Multi-hull vessels are characterized by inherent structural advantages such as improved stability, increased volumetric capacity, and enhanced operational efficiency at higher speeds. Despite these advantages, hydrodynamic optimization, particularly in terms of resistance reduction, remains a significant challenge for enhancing performance potential [1], [2]. The behavior of marine craft is primarily influenced by fluid-structure interactions, which are intensified in multi-hull systems due to interference effects arising from proximity [3], [4]. These phenomena present complicated flow-field disturbances between adjacent hulls, frequently undermining the platform's hydrodynamic efficiency despite its intrinsic features.

Interference resistance is a crucial factor influencing catamaran performance and has been extensively examined in various multi-hull configurations; however, significant gaps remain in comprehending the impact of surface roughness. Yanuar et al. [5] demonstrated that the arrangement of side hulls significantly affects interference resistance in quadramarans; however, their analysis was based on the assumption of idealized, smooth hull surfaces. This simplification neglects the hydrodynamic effects of roughness, including the modulation of the turbulent boundary layer, which can influence wave interference patterns in real-world situations. Yeung et al. [3] conducted a numerical analysis of the S60 catamaran's resistance, excluding the effects of trim and sinkage, which resulted in the oversight of dynamic interactions that may increase resistance due to roughness. Iglesias et al. [6] addressed this limitation by incorporating free trim-sinkage conditions; however, their emphasis on hull spacing did not consider the established effect of surface roughness on viscous resistance. Castiglione et al. [7] emphasized the enhancement of interference effects in shallow water. However, their conclusions are limited by the assumption of hydraulically smooth hulls, which is a notable oversight considering that turbulence induced by roughness is likely intensified in confined flow regimes. The dominance of interference resistance in catamarans is well-established, with Farkas et al. [8] and Doğrul et al. [9] identifying demi-hull section shape and separation as critical parameters. While Farkas et al. [8] linked asymmetric profiles to reduced residuary resistance, their experiments were conducted under controlled, smooth-hull conditions, limiting applicability to real-world vessels where biofouling or manufacturing imperfections alter surface topology. Doğrul et al. [9] quantified resistance increases at moderate Froude numbers ($0.3 < Fr < 0.75$) for narrow hull separations. However, their exclusion of roughness effects precludes insights into how surface texture might amplify or redistribute interference. Firdhaus et al. [10] extended this discourse to hydrofoil-supported catamarans, reporting drag penalties from foil-induced wave interactions. However, their study did not evaluate the effects of roughness foils or hulls, a critical omission given that

*CORRESPONDING AUTHOR | K. Kiryanto | ✉ kiryanto@lecturer.undip.ac.id

surface imperfections disrupt boundary layer stability and amplify viscous drag, factors particularly detrimental to hydrofoil efficiency [11].

Existing literature consistently identifies the moderate Froude regime ($0.3 < Fr < 0.75$) as a range where catamarans suffer disproportionate resistance compared to monohulls [12]. However, these findings derive from simulations and experiments that assume idealized hull smoothness, thereby ignoring the compounding effects of surface roughness. Ravenna et al. [13] addressed this gap for monohulls, demonstrating through numerical and experimental analyses that roughness increases resistance by 10–15% via turbulent skin friction and flow separation. While their work underscores the necessity of integrating surface conditions into hydrodynamic analyses, its applicability to multi-hull systems remains untested. Crucially, interference resistance in catamarans arises from synergistic wave-wave and viscous interactions between demi-hulls, a regime where roughness may uniquely perturb resistance mechanisms compared to monohulls.

Surface roughness critically influences hydrodynamic resistance in marine vessels, particularly in multi-hull systems, where it exacerbates both frictional and interference resistance [14], [15], [16], [17], [18], [19]. At the same time, catamarans derive stability and load-bearing advantages from their widely spaced hulls [20]. These benefits are counteracted by hydrodynamic interactions between hulls, which amplify resistance. Surface irregularities, such as biofouling, an inevitable consequence of marine operations, significantly increase frictional resistance, constituting 50–80% of the total drag and perturbing the flow coherence between hulls, thereby intensifying interference effects [21]. Present resistance models insufficiently account for this duality, since they separate frictional and interference resistance despite their combined deterioration under actual roughness circumstances. Biofouling may increase fuel consumption by as much as 40%, highlighting the need to include surface roughness factors into interference resistance calculations. This research directly tackles this deficiency by simulating biofouling-induced roughness to enhance prediction frameworks for optimizing catamaran performance under operational settings.

This study utilizes high-fidelity numerical simulations to systematically investigate the hydrodynamic interactions between catamaran hulls under varying surface roughness conditions, emphasizing the characterization of the synergistic relationship between roughness-induced boundary layer modifications and velocity-dependent interference effects. This study quantifies the association between surface roughness characteristics and resistance amplification across several operating speed ranges, establishing predictive relationships to guide hull design optimization. The approach provides practical insights for reducing performance decline due to biofouling and operational wear, hence enhancing strong frameworks for predicting resistance in real-world marine applications characterized by inherent surface roughness.

2. METHODS AND MATERIALS

2.1 Research Object

This work investigates the Delft 372 catamaran. The vessel's 3D model is presented in Figure 1, while Table 1 displays the principal dimensions of the ship.

Table 1. Delft 372 principal dimension [22]

Principal Dimension	Delft 372	Unit
LPP	3.000	m
Beam demihull	0.240	m
Draft	0.150	m
WSA	1.945	m^2
Displacement	87.070	kg
Cb	0.403	
S/L	0.220	m
LCG	1.410	m

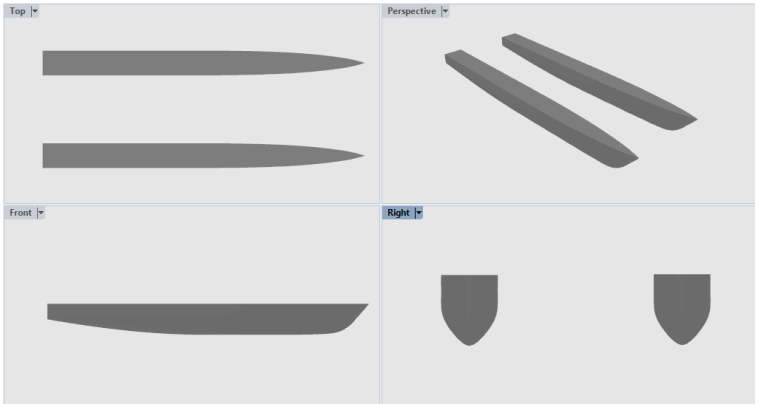

Figure 1. 3D Model Catamaran Delft 372

The modeling of the Delft 372 catamaran was carried out to accurately represent its hull geometry for computational analysis. Following the model development, the Numeca Finemarine 9.2 software was utilized to perform numerical simulations, specifically to analyze the effects of surface roughness on the ship's hull. The metrics used to ascertain surface roughness are derived from Schultz [23] under various situations. The roughness variations selected for the study, as shown in Table 2, include hydraulically smooth surfaces, anti-fouling coatings, light slime, and heavy slime. The corresponding values of equivalent sand roughness height (k_s) for these conditions were extracted from Schultz's [23] measurements and are representative of typical marine environments, reflecting various operational states a vessel may encounter during its service life. These roughness levels are particularly relevant, as they align with those used in prior research and are supported by comprehensive experimental data, providing a robust and credible foundation for our analysis.

The roughness modelling technique involves directly simulating the impact of roughness on wall boundary conditions. This may be achieved by altering the function of the wall by the direct application of roughness components. The surface roughness modelling used assumes a resemblance to sand grains (k_s), whereby the height of the sand grains serves as a benchmark for the roughness. The ship model is divided into four surface parts: the left hull, the right hull, the main deck, and the transom. However, the roughness is only represented on three surface parts: the left hull, right hull, and transom, as shown in Figure 2.

Table 2. Variation of representative fouling conditions [23]

Code	Condition description	k_s (μm)
K0	Hydraulically smooth surface	0
K1	Typical as applied AF coating	30
K2	Deteriorated coating or light slime	100
K3	Heavy slime	300

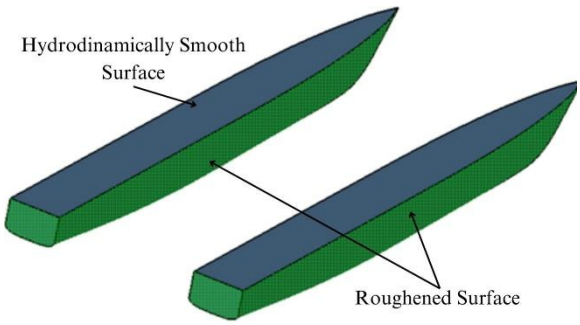

Figure 2. Surface Roughness Modeling on a 3D catamaran model

2.2 Numerical Approach

To address problems involving fluid flow, the ISIS-CFD flow solver utilizes the equations of incompressible, unsteady Reynolds-averaged Navier-Stokes (RANS). For spatially discretizing transport equations, the solution requires the use of the finite volume approach. Unstructured meshes, which may have qualities that are rotationally symmetric, two-dimensional, or three-dimensional, are discretized using the face-based technique. Diverse control volumes that do not overlap and are surrounded by diverse constitutive qualities make up these meshes. These meshes are built of separate control volumes. In the case of the flow of an incompressible multi-phase viscous fluid under isothermal circumstances, the preservation of mass, momentum, and volume fraction is determined by equations (1-3).

$$\frac{\partial}{\partial t}\int_v \rho\, dV + \int_S \rho(\mathbf{U}-\mathbf{U}_d).\mathbf{n}\, dS = 0 \tag{1}$$

$$\frac{\partial}{\partial t}\int_v \rho\, U_i dV + \int_S \rho U_i(\mathbf{U}-\mathbf{U_d}).\boldsymbol{n}\, dS = \int_S (\tau_{ij}I_j - pI_i).\mathbf{n}\, dS + \int_S \rho g_i\, dV \tag{2}$$

$$\frac{\partial}{\partial t}\int_v c_i\, dV + \int_S c_i(\mathbf{U}-\mathbf{U}_d).\mathbf{n}\, dS = 0 \tag{3}$$

A surface S that is completely enclosed, moving at a velocity $\mathbf{U}_d$ The border of the control volume V is defined by a unit normal vector n that points outward. The fields of velocity ($\mathbf{U}$) and pressure (ρ) are given. The vector I_j, there are no components other than the j component, which has a value of 1. The tensor I_j represents the viscous stress, whereas g_i Represents another variable, the gravitational vector. The determination of i fluid presence or absence may be inferred based on the value of c_i, which represents the i -th volume fraction. The computational fluid dynamics (CFD) software, NUMECA was utilized to conduct the simulations with the turbulence model of $k-\omega$ Shear Stress Transport (SST). Several key equations form the basis of its calculations [24], [25], [26], [27]. The transport equation for the turbulent kinetic energy (k), describes how turbulent kinetic energy changes over time, influenced by production, dissipation, and diffusion. This equation is expressed as follows:

$$\frac{\partial k}{\partial t} + U_j\frac{\partial k}{\partial x_j} = P_k - \beta^*\omega k + \frac{\partial}{\partial x_j}[(v+\sigma_k v_t)\frac{\partial k}{\partial x_j}] \tag{4}$$

Here, P_k Represents the production of turbulent kinetic energy, reflecting the transfer of energy from the main flow to turbulence. Meanwhile, $\beta^*\omega k$ represents the rate of dissipation of turbulent energy.

The second equation is the transport equation for the specific dissipation rate (ω), which also considers production, dissipation, and diffusion, with the addition of a particular function that allows the transition between the $k-\omega$ and $k-\varepsilon$ models:

$$\frac{\partial \omega}{\partial t} + U_j\frac{\partial \omega}{\partial x_j} = a\frac{\omega}{k}P_k - \beta\omega^2 + \frac{\partial}{\partial x_j}\left[(v+\sigma_\omega v_t)\frac{\partial \omega}{\partial x_j}\right] + 2(1-F_1\frac{\sigma_{\omega 2}}{\omega}\frac{\partial k}{\partial x_j}\frac{\partial \omega}{\partial x_j} \tag{5}$$

The function F_1 in this equation plays a crucial role in the blending process between the characteristics of the $k-\omega$ and $k-\varepsilon$ models, allowing the $k-\omega$ SST model to handle various flow conditions more effectively.

This study employs a CFD numerical simulation technique using the RANS solver with the finite volume approach. This finite volume approach employs two forms of discretization, namely in spatial and temporal domains. In the context of space, the computational domain is partitioned into a set of distinct cells, often referred to as a mesh. Similarly, the time dimension is split into a limited number of discrete time steps. The determination of timesteps is based on the recommendation of the ITTC standard formula [28] in equation (4), where L represents the ship's length overall (LOA) and U represents the ship's velocity. This yields timestep values in the range of 0.553 to 0.006, as shown in Table 3.

$$\Delta t = 0.001\sim 0.01\ \frac{L}{U} \tag{6}$$

Table 3. Timestep at each simulation speed

Fr	v (m/s)	Timestep
0.10	0.54	0.553
0.25	1.35	0.022
0.50	2.71	0.011
0.65	3.52	0.008
0.80	4.34	0.006

2.3 Boundary Conditions and Meshing

The computational domain, as shown in Figure 3 and Table 4, incorporates boundary conditions derived from the ITTC Recommended Procedures and Guidelines for Computational Fluid Dynamics (CFD) ship Resistance [28]. These boundary conditions were carefully selected to reflect realistic operational conditions and ensure the accuracy of the simulation. The inlet was placed one times the ship's length (L) upstream, and the outlet was positioned three times the ship's length (L) rearward, ensuring a sufficient flow domain for accurate results. The sidewalls were set 1.5 times the ship's length (L) away from the waterline. At the same time, the same free-stream far-field velocity was applied to the sidewall, outlet, and inlet to maintain consistency across the boundaries. The bottom and upper walls were positioned 1.5 times the length (L) below and equal to the length above the model, respectively, with constant pressure defined to simulate typical environmental conditions. To ensure zero slip at the hull, a wall function was employed as the boundary

condition. These boundary setups were chosen based on industry standards and previous studies to provide a reliable and representative physical setup for the simulation. Additionally, the simulations accounted for and rectified any rotational and vertical motions, further improving the accuracy of the results.

Table 4. Boundary condition setup

Boundary Condition	Description
Inlet	Free stream far-field velocity
Outlet	Free stream far-field velocity
Sidewall	Free stream far-field velocity
Bottom Wall	Constant pressure defined
Upper Wall	Constant pressure defined
Ship's Hull	Wall function

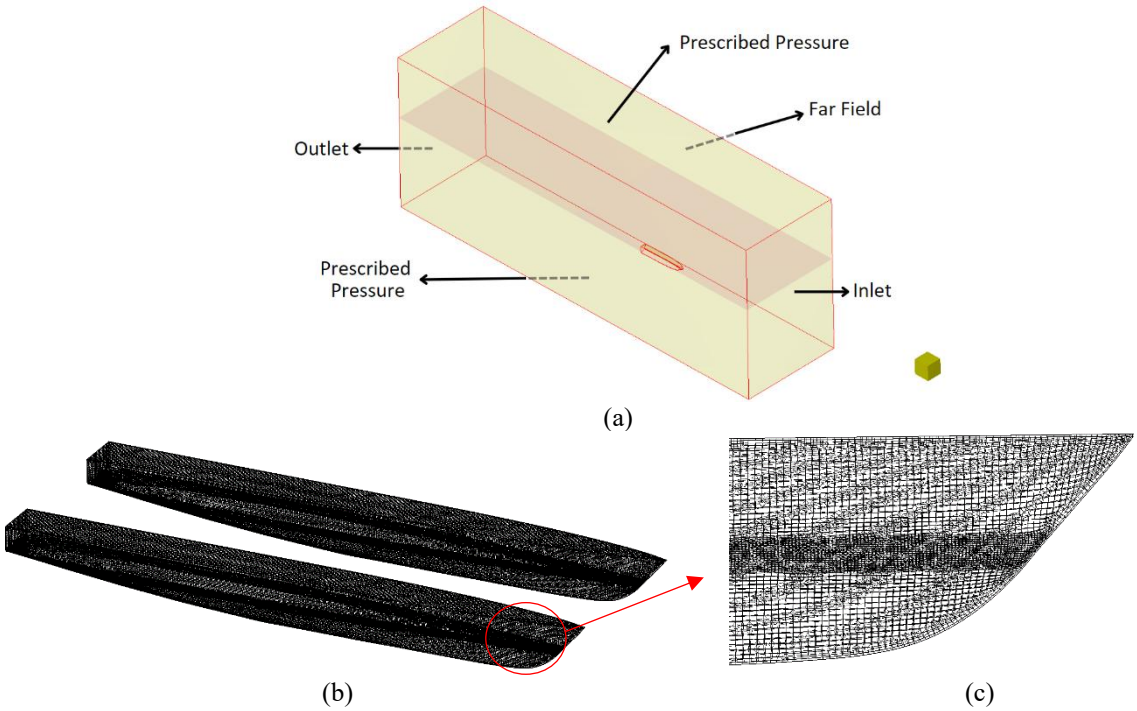

Figure 3. The computational domain and boundary conditions are shown in the simulation model (a), while the surface of the simulation model is represented by the detailed mesh (b)

In the area where the wall's viscosity significantly affects the turbulent zone, the wall distance (Y+) is used. Using the local viscous length scale as a standard, Y+ is the dimensionless distance from the first grid node to the surface of the wall. According to the 2011 International Towing Tank Conference (ITTC), the Y+ value ought to range anywhere between 30 and 100 [29]. The following formula is used to compute the following: Figure 4 displays the ship's Y+ value, which generally ranges between 45 and 75.

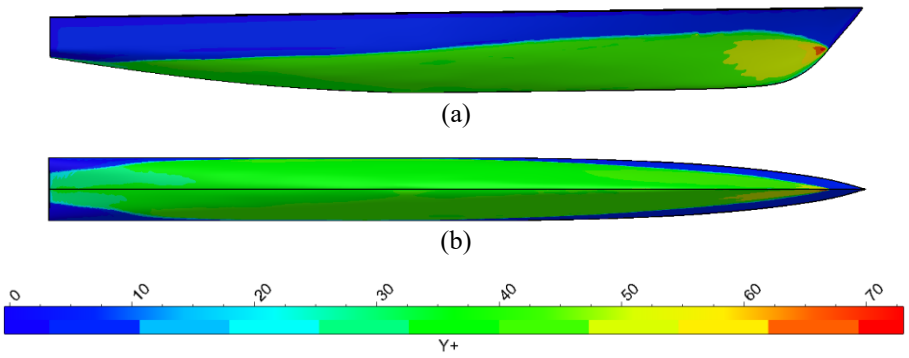

Figure 4. Wall Y+ on Delft 372 Catamaran at Fr = 0.80

3. RESULTS AND DISCUSSION

3.1 Verification and Validation

A systematic grid convergence analysis was conducted to ensure numerical accuracy and computational efficiency, evaluating six mesh configurations (0.33×10^6 to 4.98×10^6 cells) under consistent hydrodynamic conditions (Fr 0.5). Total resistance (R_T) served as the convergence metric, with refinement increments of 1.5–2.5× cell counts to isolate discretization errors [30]. Results shown in Table 5 and Figure 5 demonstrate asymptotic R_T stabilization beyond 0.62×10^6 cells, where further refinement to 1.24×10^6 cells produced a marginal 0.39% deviation—below the 1% engineering significance threshold—while increasing computational runtime by 320%. The 1.24×10^6 cells mesh was selected as optimal, capturing 99.69% of the converged solution with 12-hour runtime efficiency, balancing numerical fidelity and resource utilization.

The mesh type obtained from the 4th simulation is then chosen and merged with the ship type, which is determined by the speed used. To validate the precision of the outcomes, the results obtained from the CFD simulation were compared with empirical data collected from prior investigations. This study primarily investigated the process validation parameter known as the interference factor (IF). The following section will discuss additional components, including overall ship resistance, the overall ship resistance coefficient, and wave elevation. An analysis of CFD and Experimental Fluid Dynamics (EFD) findings indicates significant discrepancies across various velocity levels.

Table 5. Value of expanding mesh cells at the same vs. simulation for mesh convergence

Run i-th	Cells Amount	R_T (N)	Error (%)
1	0.33×10^6	1.32	
2	0.41×10^6	1.30	1.72%
3	0.62×10^6	1.29	0.95%
4	1.24×10^6	1.28	0.46%
5	2.48×10^6	1.28	0.39%
6	4.98×10^6	1.28	0.31%

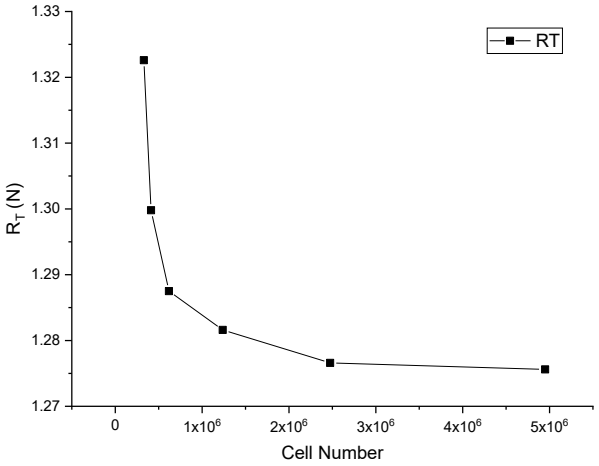

Figure 5. Function of the number of cells on the ship's resistance at constant speed (Fr 0.5)

According to the data in Table 6 and Figure 6, the results of CFD calculations on EFD by Broglia et al. [33] show that the lowest deviation value is 0.85% for the low-speed catamaran Fr 0.1. In comparison, the most significant deviation is 6.27% for the high-speed Fr 0.8. The disparity in deviation arises from the comparison between two distinct methodologies: EFD calculation results and CFD numerical findings. This discrepancy is mainly attributed to the constraints in accurately modelling the environment to match actual experimental settings. The resistance prediction is deemed satisfactory as the average absolute error value remains below 10%, which is regarded as acceptable for resistance simulations. The verification and validation calculations are shown in Table 6.

Table 6. Comparison of Delft 372 catamaran EFD [31] and CFD ship resistance

Fr	Vs (ms)	EFD (N)	CFD (N)	Deviation (%)
0.10	0.54	1.26	1.27	0.85
0.25	1.35	7.81	7.68	1.68
0.50	2.71	50.02	48.21	3.61
0.65	3.52	67.87	64.21	5.41

0.80	4.34	89.51	83.90	6.27

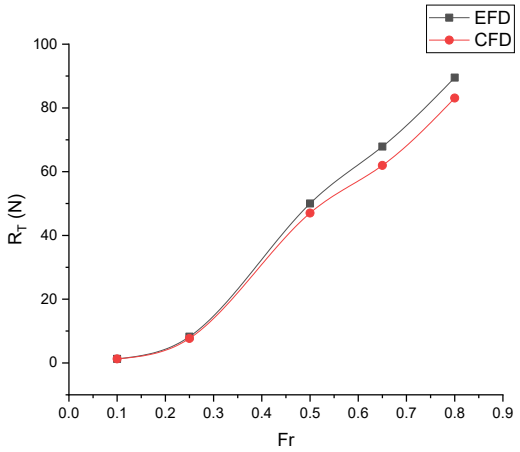

Figure 6. Ship resistance (R_T) as a function of ship Froude number (Fr) of CFD and EFD measurement by Broglia et al. [31]

3.2 Total Ship Resistance

This section presents the results of the CFD simulation about the total resistance of the catamaran. The simulations entail modelling the Delft-372 catamaran, which includes a hydraulically smooth base model (K0) and three supplementary catamaran models (K1-K3) that demonstrate differing levels of roughness. The simulations are performed at five distinct speeds, varying from Fr 0.1 to 0.8, to determine the ship's total resistance. The simulation produces the total resistance of the ship, denoted as R_T.

Figure 7 illustrates the correlation between ship velocity (Fr) and overall ship resistance (N) for four distinct surface conditions: a hydrodynamically smooth surface (K0), a surface treated with an anti-fouling coating (K1), a surface with a thin layer of slime (K2), and surfaces with a thick layer of slime (K3). The simulation was conducted at a range of velocities from Fr 0.1 to 0.8. The findings indicate that overall resistance rises in tandem with the increase in speed across all situations. K0 exhibits the most minimal resistance, whereas K1, K2, and K3 show progressively higher levels of resistance. The surface coated with a thick layer of slime (K3) exhibits the most significant level of resistance, while the sleek and streamlined hydrodynamic surface (K0) displays the lowest level of resistance. Based on the graph, it can be inferred that the overall resistance of the ship rises with an increase in the roughness of its surface. Rough surfaces, such as those covered in thick slime, result in a substantial rise in drag, reaching up to 35% at maximum speed (Fr 0.8). Conversely, smoother surfaces, such as those treated with anti-fouling, lead to reduced drag. These findings are consistent with and corroborate the results of earlier studies by Hakim et al. [32]. Additionally, the EFD measurements by Broglia et al. [31] were included as a benchmark for comparison, further validating our simulation results. The EFD data provided a solid reference for verifying the accuracy of our CFD simulations, reinforcing the credibility of our conclusions regarding the effects of surface roughness on ship resistance.

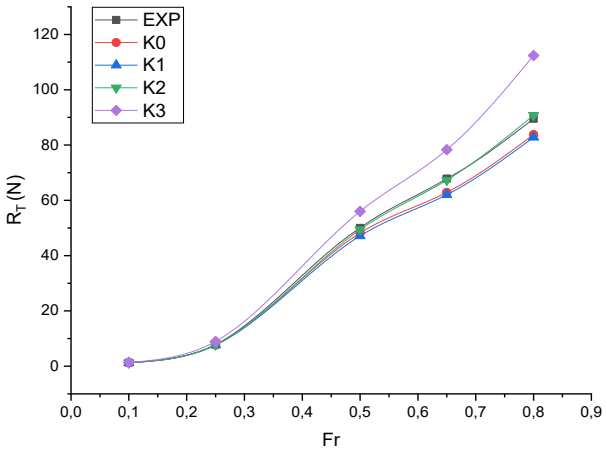

Figure 7. Ship resistance (RT) as a function of ship Froude number (Fr) of 4 different surface roughness conditions and EFD measurement by Broglia et al. [31]

3.3 Wetted Surface Area

This section provides the findings of the CFD simulation on the wetted surface area (WSA) of the catamaran. The wetted surface area of the Delft-372 catamaran and its four modifications (K0-K3) with different roughness levels are

simulated at five speeds (Fr 0.1 to 0.8) to calculate their respective surface areas. The simulation yields the wetted surface area of the ship, designated as WSA.

Figure 8 illustrates the outcomes of a simulation examining the Wetted Surface Area (WSA) of a catamaran at various speeds, ranging from Fr 0.1 to 0.8, with varying degrees of surface roughness. For a hydrodynamically smooth surface (K0), shown by the black line with squares, the WSA is minimal, indicating the lowest resistance to water flow. The surface, shown by a red line with circles, demonstrates an increased WSA attributable to the roughness of the anti-fouling coating (K1), indicating improved resistance to fouling. The surface of the light slime (K2), shown by a blue line with triangles, has a markedly increased WSA due to the presence of a thin layer of microorganisms. The K3 slime's surface is distinguished by a thick layer, as shown by a green line adorned with stars. It has the greatest WSA, with a significant increase of 1.24% relative to K0. This indicates robust resistance to the proliferation of dense bacteria on this surface. The WSA typically escalates with vessel velocity across all surface categories. Smoother surfaces exhibit lower WSA, thereby enhancing hydrodynamic efficiency. Conversely, rough surfaces or those affected by biofouling (e.g., coatings and slime) experience increased WSA and frictional resistance, consequently reducing operating efficiency, as observed by Hakim et al. [33]. These findings highlight the crucial role of surface characteristics and roughness in optimizing ship performance through effective design and maintenance strategies.

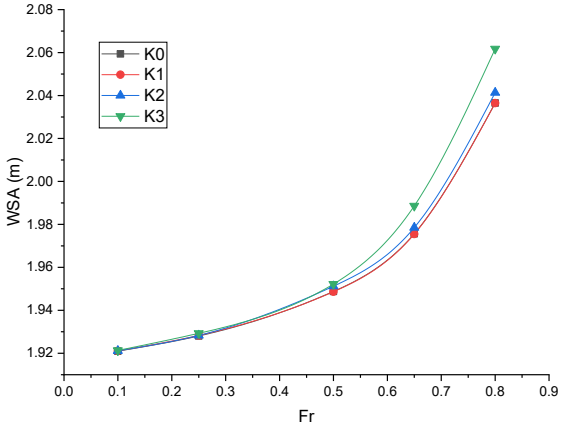

Figure 8. Wetted surface area (WSA) as a function of the ship Froude number (Fr) of 4 different surface roughness conditions

3.4 Total Ship Resistance Coefficient

The total drag coefficient, denoted as C_T, is a dimensionless coefficient that represents the ratio of the total drag to half the density of water, the surface area of the hull immersed in water, and the square of the ship's speed. The C_T The formula is defined by equation (5), which is as follows:

$$C_T = \frac{R_T}{1/2\, v^2 \rho WSA} \tag{7}$$

C_T represents the overall resistance coefficient of the ship, R_T Represents the total resistance of the ship in Newtons (N), v represents the speed of the vessel in meters per second (m/s), ρ represents the density of seawater, which is 1025 kilograms per cubic meter (kg/m^3), and WSA represents the wet surface area of the ship's hull in square meters (m^2).

The analysis of variations in the catamaran total drag coefficient, as shown in Figure 9, reveals that the total drag coefficient at low speed (Fr 0.1) decreases with increasing surface roughness. However, in the speed range of Fr 0.25 – 0.65, there is an increase in the catamaran drag coefficient value. At high speeds, Fr 0.8, the catamaran's overall drag coefficient tends to rise as surface roughness increases. The catamaran with a roughness of 300 µm (K3) had the most significant total drag coefficient value at a speed of Fr 0.5, while the monohull with a roughness of 0 µm achieved the least total drag coefficient value at a speed of Fr 0.25. The data indicate a significant rise in the overall drag coefficient of the catamaran, up to 23%, as the speed increases from Froude number 0.25 to Froude number 0.5. There is a substantial drop in value on catamarans as the speed rises from Fr 0.5 to Fr 0.65, accompanied by an increase in surface roughness. However, there is a consistent fall in value throughout the speed range of Fr 0.5 to Fr 0.65 to Fr 0.8 as surface roughness increases.

The overall drag coefficient is significantly affected by the total resistance value, vessel speed, and the submerged surface area of the hull. This is due to the computation supposing that the hull's submerged surface area is in the original static state. Conversely, in this CFD numerical computation, the surface area is used subsequent to its immersion in water. Simulations are performed to depict surface roughness, which significantly influences the resistance and surface area of a ship's hull in numerical analysis.

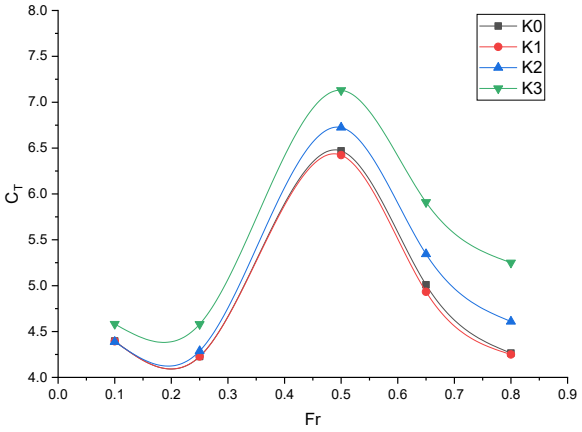

Figure 9. Total resistance coefficient (C_T) as a function of ship Froude number (Fr) of 4 different surface roughness conditions

3.5 Interference Factor

The interference factor is a value that determines the effect on the drag of the catamaran due to the interaction between the two hulls. The interference factor is defined as the relative difference between the total drag coefficient of a catamaran and a monohull by the formula:

$$IF = \frac{C_T^C - C_T^M}{C_T^M} \tag{8}$$

The interference factor, denoted as IF, represents the effect of interference on the drag of a catamaran. C_T^C refers to the overall drag coefficient of the catamaran, whereas C_T^M Represents the total drag coefficient of the monohull.

Figure 10 presents the computed interference factor (IF) across Froude numbers (Fr) and four surface roughness conditions. The IF quantifies hydrodynamic interactions between catamaran demihulls: *negative values* indicate favorable interference (total catamaran resistance lower than two monohulls), while *positive values* denote adverse interference (higher resistance). At low speeds (Fr ≤ 0.25), IF approaches zero across all surfaces, suggesting negligible interaction effects. A pronounced unfavorable peak (IF > +0.15) occurs at Fr ≈ 0.5, particularly for smoother surfaces (30 µm and hydrodynamically smooth). Beyond Fr 0.65, IF declines sharply, culminating in negative values at Fr 0.8 for rougher surfaces (e.g., −0.08 at 300 µm). This trend aligns with Broglia et al. and Zaghi et al.'s experimental observations [31], [34], further supporting the observed trends in hydrodynamic interactions.

The transition to negative interference factor (IF) values at high speeds (Fr 0.8) exhibits a strong correlation with surface roughness. Specifically, the most favorable IF observed (–0.08) occurred at Fr 0.8 under the roughest surface condition (300 µm average height), contrasting sharply with the least favorable IF (+0.15) recorded at Fr 0.5 on smoother surfaces (30 µm and hydrodynamically smooth). This inverse relationship between roughness and IF at high Froude numbers suggests that surface texture critically alters hydrodynamic behavior through two primary mechanisms: flow separation dynamics and wave interference modulation. Mechanistically, increased surface roughness promotes early transition to turbulence within the boundary layer, delaying laminar separation and subsequently reducing wave-making resistance. Concurrently, roughness modifies phase interactions between demihull wave systems, diminishing constructive wave interference that typically elevates resistance at medium speeds. A third contributing factor involves enhanced momentum transfer near the transom region, where accelerated turbulent energy dissipation reduces viscous pressure resistance. These phenomena collectively explain the observed inversion from unfavorable to favorable interference at high speeds on rough surfaces.

Thus, catamarans generally demonstrate positive interference factors (unfavorable), whereas high-speed operations on rough surfaces may result in negative interference factors (favorable). At Fr 0.8, rough surfaces (300 µm) produced negative IF, signifying a decrease in net resistance. Conversely, low speeds (Fr 0.1–0.25) demonstrated near-zero IF (marginally unfavorable), while medium speeds (Fr 0.5–0.65) displayed positive IF (detrimental). The dependency of speed on roughness was consistent across all tested surfaces.

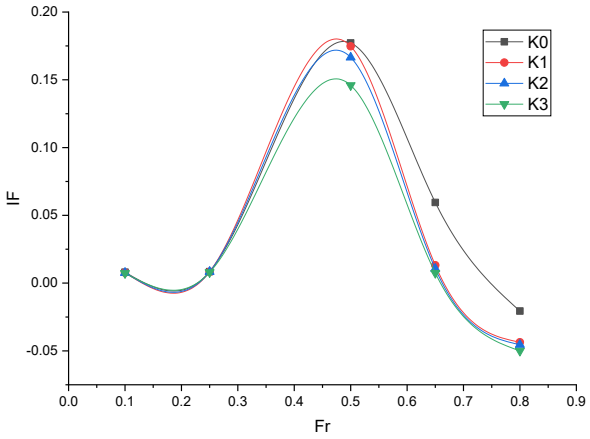

Figure 10. Interference Factor (IF) as a function of ship Froude number (Fr) of 4 different surface roughness conditions

3.6 Wave Elevation

Wave pattern refers to the intricate flow pattern of waves between the two hulls of a catamaran. The flow patterns of these waves spread from the bow to the stern of the ship at Fr 0.5, and the focus of this discussion is on the interference resistance patterns that occur between the two hulls of the ship. The wave profile is represented as contour lines of the free surface elevation, each shown in Figure 11(a). Subsequently, cross-sectional wave elevations were measured at coordinates (a) and (b), the results of which are presented in Figures 11(b) and 11(c).

Figures 11(b) and 11(c) provide graphic representations of the wave heights produced at the stern region of the ship and the space between the hulls, respectively. The findings shown in Figure 11(b) indicate that augmenting the surface roughness of the Delft 372 catamaran has little impact on the wake generated during the ship's motion. The effect of surface roughness on the Delft 372 catamaran is evident in Figure 11(c), as it displays a noticeable variation in wave height. Stern wave patterns, as shown in Figure 11(b), demonstrate behavior that is largely insensitive to surface roughness, primarily due to the dominance of flow separation, which contributes to more than 90% of the wave-making resistance. In contrast, inter-hull wave profiles (Figure 11(c)) exhibit substantial modulation due to surface roughness, where the application of anti-fouling coating (K1) enhances constructive interference, achieving a peak value of 0.193 meters. Conversely, heavy slime (K3) mitigates wave resonance by promoting premature flow separation, resulting in a 14.5% reduction in wave height (0.165 meters). Light slime (K2), on the other hand, induces turbulent dissipation.

This observed divergence in behavior highlights two key points: Stern hydrodynamics align with the autonomy principle outlined by Ravenna et al. [13], wherein inviscid pressure fields are largely unaffected by boundary layer conditions, and Inter-hull interference is significantly altered by roughness, primarily through mechanisms that disrupt coherent pressure gradients essential for wave superposition. As a result, the viscous penalty of K3 outweighs the potential reduction in wave resistance at Froude number 0.5. Conversely, the interference amplification observed with K1 optimizes wave-making efficiency despite the associated fouling risks. These findings underscore the importance of surface conditioning in managing interference zones while indicating that it has minimal impact on stern-dominated resistance.

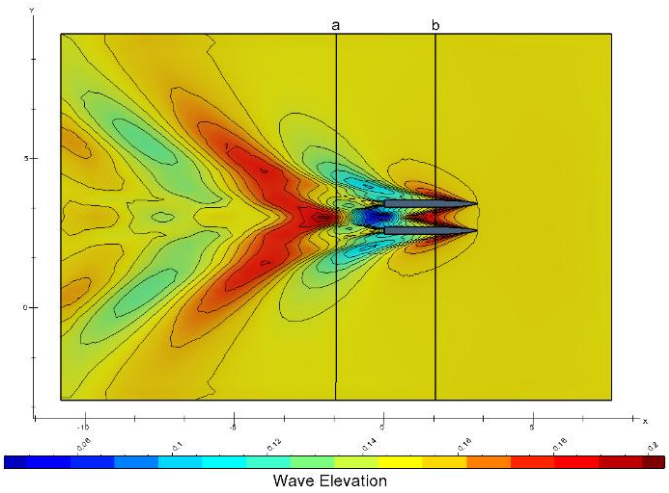

(a)

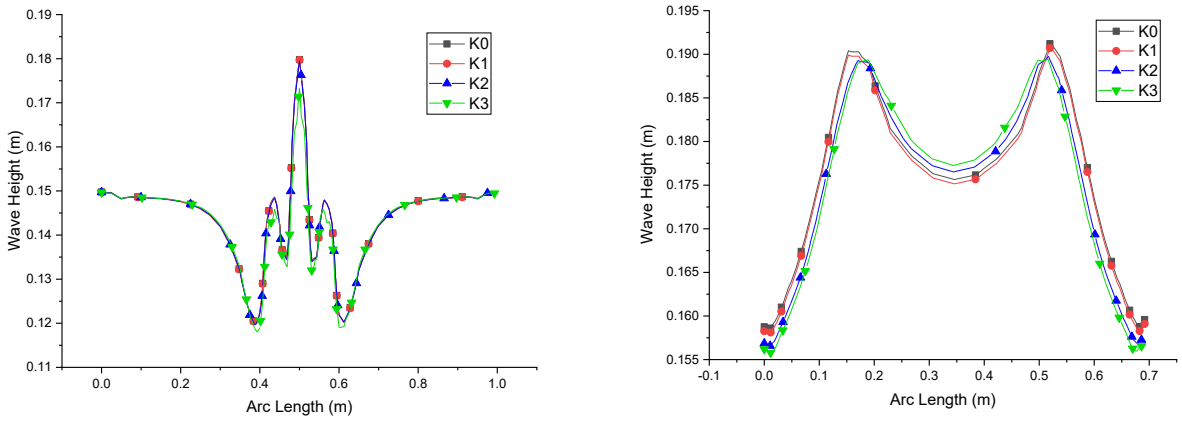

Figure 11. (a) visualization of the free surface pattern on the catamaran at a speed of Fr 0.5, (b) wave height pattern in the area behind the catamaran at a speed of Fr 0.5 at coordinates a-a, (c) wave height pattern in the area between the hulls of the catamaran at a speed of Fr 0.5 at coordinate b-b

4. CONCLUSIONS

This investigation quantitatively evaluated the hydrodynamic consequences of biofouling-induced surface roughness on catamaran performance across the operational ship speed, addressing a fundamental gap in predicting interference effects under realistic fouling conditions. Through validated RANS-based computational fluid dynamics employing a k-ω SST turbulence model, four surface conditions were systematically examined: hydrodynamically smooth (K0), anti-fouling coating (K1), light slime (K2), and heavy slime (K3). Key findings establish a speed-dependent roughness interaction paradigm. Surface roughness consistently elevated total resistance, with heavy biofouling (K3) inducing 35% greater ship resistance at Fr 0.8 relative to hydrodynamically smooth surfaces (K0). Conversely, a paradoxical high-speed phenomenon emerged: at Fr 0.8, 300 μm roughness generated favorable interference, IF = -0.08, through turbulence-mediated wave suppression, while hydraulically smooth surfaces exhibited peak detrimental interference, IF 0.15, at Fr 0.5 due to constructive wave reinforcement. Wave elevation analysis further demonstrated a 14.5% reduction in inter-hull wave amplitude for K3 versus K1 at Fr 0.5, whereas stern wave profiles remained roughness-insensitive owing to flow-separation dominance. The wetted surface area expanded by 1.24% under heavy fouling, exacerbating frictional resistance despite the attenuation of wave-making components.

These results resolve the biofouling paradox through three identified compensatory mechanisms: premature boundary layer transition, which delays laminar separation; disruption of constructive wave superposition; and enhanced turbulent momentum transfer, which reduces viscous pressure resistance. Consequently, while fouling invariably increases viscous drag, it confers net resistance reduction at Fr ≥ 0.65 when wave-making suppression dominates skin friction penalties. This challenges traditional beliefs on universal biofouling, demonstrating that effective hydrodynamic management requires focused fouling removal in the bow or midship areas, where roughness exacerbates wave interference, whereas stern parts are hardly impacted. This study introduces a mechanistic, speed-dependent approach for catamaran design in fouling situations, demonstrating that deliberate control of roughness, rather than universal reduction, may improve high-speed efficiency. This signifies a fundamental shift in hydrodynamic optimization for maritime operations, with significant consequences for sustainable vessel maintenance and performance forecasting.

This work has several limitations, notably the biofouling represented as static uniform roughness, which overlooks dynamic factors such as slime oscillation or viscoelastic biofilm behavior. Moreover, RANS simulations using k-ω SST models may underestimate anisotropic turbulence in separated flows, especially for vortex shedding generated by roughness. These limits underscore prospects for forthcoming high-fidelity investigations within expanded operating parameters.

ACKNOWLEDGEMENTS

This research was financed by funding other than the State Revenue and Expenditure Budget (excluding the APBN) of Diponegoro University for the Fiscal Year 2024, under contract number 606-96/UN7.D2/PP/VII/2024.

CONFLICT OF INTEREST

The authors have conducted a comprehensive review and verified that there are no conflicts of interest regarding the results and materials presented in this work.

AUTHORS CONTRIBUTION

A. Firdhaus (Conceptualisation; Methodology; Validation)

K. Kiryanto (Supervision; Funding acquisition)

A. F. Zakki (Formal analysis; Investigation)

M. L. Hakim (Writing - review & editing)

H. Khalis (Writing - original draft)

REFERENCES

[1] A. Fitriadhy, S. A. Azmi, N. Aqilah Mansor, and N. Adlina Aldin, "Computational fluid dynamics investigation on total resistance coefficient of a high-speed "deep-V" catamaran in shallow water," *International Journal of Automotive and Mechanical Engineering*, vol. 14, no. 2, pp. 4369–4382, 2017.

[2] R. W. Yeung and H. Wan, "Multi-hull and surface-effect ship configuration design: A framework for powering minimization," *Journal of Offshore Mechanics and Arctic Engineering*, vol. 130, no. 3, p. 031005, 2008.

[3] R. Yeung, G. Poupard, J. O. Toilliez, H. Söding, A. S. Gotman, and H. F. Hemmen, "Interference-resistance prediction and its applications to optimal multi-hull configuration design," *Transactions - Society of Naval Architects and Marine Engineers*, vol. 112, pp. 142–169, 2005.

[4] A. Aubault and R. W. Yeung, "Interference resistance of multi-hull vessels in finite-depth waters," in *Volume 4: Offshore Geotechnics; Ronald W. Yeung Honoring Symposium on Offshore and Ship Hydrodynamics*, American Society of Mechanical Engineers, pp. 721–730, 2012.

[5] Yanuar, Ibadurrahman, S. Karim, and M. Ichsan, "Experimental study of the interference resistance of pentamaran asymmetric side-hull configurations," in *AIP Conference Proceedings*, American Institute of Physics Inc., vol. 1826, no. 1, p. 020025, 2017.

[6] A. Souto-Iglesias, D. Fernández-Gutiérrez, and L. Pérez-Rojas, "Experimental assessment of interference resistance for a Series 60 catamaran in free and fixed trim-sinkage conditions," *Ocean Engineering*, vol. 53, pp. 38–47, 2012.

[7] T. Castiglione, W. He, F. Stern, and S. Bova, "URANS simulations of catamaran interference in shallow water," *Journal of Marine Science and Technology*, vol. 19, no. 1, pp. 33–51, 2014.

[8] A. Farkas, N. Degiuli, I. Tomljenović, and I. Martić, "Numerical investigation of interference effects for the Delft 372 catamaran," *Proceedings of the Institution of Mechanical Engineers, Part M: Journal of Engineering for the Maritime Environment*, vol. 238, no. 2, pp. 385–394, 2023.

[9] A. Doğrul, E. Kahramanoğlu, and F. Çakıcı, "Numerical prediction of interference factor in motions and added resistance for Delft catamaran 372," *Ocean Engineering*, vol. 223, p. 108687, 2021.

[10] A. Firdhaus, K. Kiryanto, G. Rindo, and A. Trimulyono, "Analysis of interference factor in hydrofoil-supported catamarans (HYSUCAT)," *Kapal: Jurnal Ilmu Pengetahuan dan Teknologi Kelautan*, vol. 21, no. 1, pp. 1–9, 2024.

[11] S. Song, Y. K. Demirel, C. De Marco Muscat-Fenech, T. Sant, D. Villa, T. Tezdogan, et al., "Investigating the effect of heterogeneous hull roughness on ship resistance using CFD," *Journal of Marine Science and Engineering*, vol. 9, no. 2, p. 202, 2021.

[12] M. Insel and A. F. Molland, "An investigation into the resistance components of high speed displacement catamarans," PhD dissertation, University of Southampton, 1990.

[13] R. Ravenna, A. Marino, S. Song, Y. Demirel, M. Atlar, and O. Turan, "Experimental investigation on the effect of biomimetic tubercles on the hydrodynamics of a flat plate," in *6th International Conference on Advanced Model Measurements Technologies for The Maritime Industry (AMT'19)*, 2019.

[14] I. K. A. P. Utama, I. K. Suastika, and M. L. Hakim, "The phenomenon of friction resistance due to streamwise heterogeneous roughness with modified wall-function RANSE," in *Applications of Computational Fluid Dynamics Simulation and Modeling*, IntechOpen, 2022.

[15] S. Song, S. Dai, Y. K. Demirel, M. Atlar, S. Day, and O. Turan, "Experimental and theoretical study of the effect of hull roughness on ship resistance," *Journal of Ship Research*, vol. 65, no. 1, pp. 62–71, 2021.

[16] W. Amiruddin *et al.*, "Prediction of the impact of biofouling roughness on a full-scale planing boat performance using CFD," *Ocean Engineering*, vol. 301, p. 117457, 2024.

[17] A. Firdhaus, P. Manik, M. L. Hakim, and K. Kiryanto, "CFD analysis of the influence of marine fouling on the performance of high-speed planning craft," *Journal of Advanced Research in Fluid Mechanics and Thermal Sciences*, vol. 110, no. 2, pp. 124–137, 2023.

[18] M. L. Hakim, B. Nugroho, T. Putranto, K. Suastika, and I. K. A. P. Utama, "Assessment of drag penalty resulting from the roughness of freshly cleaned and painted ship-hull using computational fluid dynamics," *11st International Conference on Marine Technology MARTEC 2018*, 2018.

[19] M. L. Hakim, B. Nugroho, M. N. Nurrohman, I. K. Suastika, and I. K. A. P. Utama, "Investigation of fuel consumption on an operating ship due to biofouling growth and quality of anti-fouling coating," *IOP Conf Ser Earth Environ Sci*, vol. 339, no. 1, 2019.

[20] H. Kawashima, H. Mieno, T. Hiroi, and T. Hamada, "Effect of Roughness Shape Parameter of Painted Surface on Frictional Resistance," in *Practical Design of Ships and Other Floating Structures*, T. Okada, K. Suzuki, and Y. Kawamura, Eds., Singapore: Springer Singapore, pp. 227–245, 2021.

[21] Y. K. Demirel, O. Turan, and A. Incecik, "Predicting the effect of biofouling on ship resistance using CFD," *Applied Ocean Research*, vol. 62, pp. 100–118, 2017.

[22] C. Gallin, "Inventiveness in Ship Design," *TU Delft, Faculty of Marine Technology, OEMO, Published in: North East Coast Institution of Engineers and Shipbuilders, Bolbec Hall, Newcastle upon Tyne, UK*, Oct. 1977, Accessed: May 30, 2022. [Online]. Available: http://resolver.tudelft.nl/uuid:94565129-2c80-4504-9414-68f2494a9218

[23] M. P. Schultz, "Effects of coating roughness and biofouling on ship resistance and powering," *Biofouling*, vol. 23, no. 5, pp. 331–341, 2007.

[24] F. R. Menter, "Two-equation eddy-viscosity turbulence models for engineering applications," *AIAA Journal*, vol. 32, no. 8, pp. 1598–1605, 1994.

[25] F. R. Menter, "Influence of freestream values on k-omega turbulence model predictions," *AIAA Journal*, vol. 30, no. 6, pp. 1657–1659, 1992.

[26] F. Menter, "Zonal two equation k-w turbulence models for aerodynamic flows," in *23rd Fluid Dynamics, Plasmadynamics, and Lasers Conference*, in Fluid Dynamics and Co-located Conferences, American Institute of Aeronautics and Astronautics, 1993.

[27] F. R. Menter, "Performance of popular turbulence model for attached and separated adverse pressure gradient flows," *AIAA Journal*, vol. 30, no. 8, pp. 2066–2072, 1992.

[28] ITTC, "Recommended Procedures and Guidelines Practical Guidelines for Ship Resistance CFD," 2014.

[29] ITTC, "Recommended Procedures and Guidelines Practical Guidelines for Ship CFD Applications," 2011.

[30] John. D. Anderson, *Computational Fluid Dynamics; The Basic With Applications*. 1995.

[31] R. Broglia, B. Jacob, S. Zaghi, F. Stern, and A. Olivieri, "Experimental investigation of interference effects for high-speed catamarans," *Ocean Engineering*, vol. 76, pp. 75–85, 2014.

[32] M. L. Hakim, B. Nugroho, I. K. Suastika, and I. K. A. P. Utama, "Alternative empirical formula for predicting the frictional drag penalty due to fouling on the ship hull using the design of experiments (DOE) method," *International Journal of Technology*, vol. 12, no. 4, pp. 829–842, 2021.

[33] M. L. Hakim, B. Nugroho, R. C. Chin, T. Putranto, I. K. Suastika, and I. K. A. Pria Utama, "Drag penalty causing from the roughness of recently cleaned and painted ship hull using RANS CFD," *CFD Letters*, vol. 12, no. 3, pp. 78–88, 2020.

[34] S. Zaghi, R. Broglia, and A. Di Mascio, "Experimental and numerical investigations on fast catamarans interference effects," *Journal of Hydrodynamics*, vol. 22, no. 5 SUPPL. 1, pp. 528–533, 2010.